Glyphs for General Second-Order 2D and 3D Tensors

Tim Gerrits, Christian Rössl, and Holger Theisel

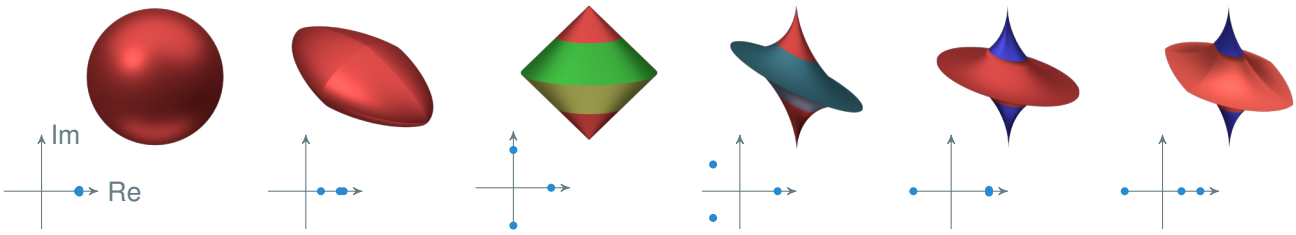

Fig. 1: Glyphs for different general second-order 3d tensors together with their eigenvalues plotted in the complex plane.

Abstract—Glyphs are a powerful tool for visualizing second-order tensors in a variety of scientic data as they allow to encode physical behavior in geometric properties. Most existing techniques focus on symmetric tensors and exclude non-symmetric tensors where the eigenvectors can be non-orthogonal or complex. We present a new construction of 2d and 3d tensor glyphs based on piecewise rational curves and surfaces with the following properties: invariance to (a) isometries and (b) scaling, (c) direct encoding of all real eigenvalues and eigenvectors, (d) one-to-one relation between the tensors and glyphs, (e) glyph continuity under changing the tensor. We apply the glyphs to visualize the Jacobian matrix fields of a number of 2d and 3d vector fields.

Index Terms—Glyph-based Techniques, Tensor Field Data, Flow Visualization

1 Introduction

Glyphs are omnipresent in Scientific Visualization. Whenever multidimensional information is to be visualized at a certain location in data space or screen space, glyphs are the standard choice. For multidimensional data of a certain type, there is generally not one best glyph. Rather a number of design decisions are possible that are based on either general or application specific design rules [1].

In this paper, we search for glyphs for *general* second-order tensors in 2d and 3d, i.e., tensors that are *not* necessarily symmetric. Such tensors appear in a variety of applications, e.g., in computational fluid dynamics and flow visualization as the Jacobian matrix of velocity fields or as stress tensors in mechanical engineering. General second-order tensors are considered as general matrices in $\mathbb{R}^{2\times 2}$ or $\mathbb{R}^{3\times 3}$ without constraints like symmetry, i.e., the space of all such tensors has 4 or 9 dimensions, respectively.

2 A Wish List of Glyph Properties

Meaningful glyphs for general second-order tensors must satisfy a number of requirements. In this section, we collect and motivate desired properties of glyphs. Let $\mathbf{J}$ be a general 2d or 3d tensor represented by a – not necessarily symmetric – matrix, and let $G(\mathbf{J})$ be its corresponding glyph. We stick to the interpretation of a tensor as the Jacobian of a vector field and thus use the symbol $\mathbf{J}$ throughout the paper. Nevertheless, the proposed properties are general and apply to any interpretation or application of tensors.

(a) *Invariance under isometric domain transformation.* Let $\mathbf{Q}$ denote an isometric map, e.g., rotation or reflection, as an orthogonal matrix. Then the domain transformation of the tensor should result in the same transformation of the glyph.

$$G(\mathbf{Q}\mathbf{J}\mathbf{Q}^{\mathrm{T}}) \;=\; \mathbf{Q}G(\mathbf{J})\,. \tag{1}$$

(b) *Scaling invariance.* A uniform scaling of the tensor should result in the same scaling of the glyph, i.e., for any $s > 0 \in \mathbb{R}$

$$G(s\,\mathbf{J}) = s\,G(\mathbf{J})\,.$$

(c) *Direct encoding of real eigenvalues and eigenvectors.* If $\mathbf{J}$ has real eigenvalues and eigenvectors, they should be directly visible in the glyph. This is justified by the fact that the eigenvalues and eigenvectors capture all information of the tensor. If they are all real-valued, they provide geometric information that is suitable for direct visualization: direction of eigenvectors and magnitude of eigenvalues. This is the case for symmetric tensors with orthogonal eigenvectors and also for a class of non-symmetric tensors with real-valued but non-orthogonal eigenvectors.

(d) *Uniqueness.* Obviously, a tensor $\mathbf{J}$ should result in a unique glyph. We also demand the reverse: a glyph should have a unique tensor. For any two tensors $\mathbf{J}_1, \mathbf{J}_2$ we demand

$$\mathbf{J}_1 \neq \mathbf{J}_2 \quad \Rightarrow \quad G(\mathbf{J}_1) \neq G(\mathbf{J}_2)\,. \tag{2}$$

We introduce *weak uniqueness* that requires (2) only for tensors of full rank, i.e., for two lower-rank tensors may "share" the same glyph.

(e) *Continuity.* Continuous changes of the tensor must result in continuous changes of the glyph. In particular, there should be no instantaneous change of the glyph appearance for a small change of the tensor. This includes the transition from positive to negative determinant, from orthogonal to non-orthogonal real eigenvectors, from distinct to multiple eigenvalues, and from real to complex eigenvalues.

$$\mathbf{J}_1 \approx \mathbf{J}_2 \quad \Rightarrow \quad G(\mathbf{J}_1) \approx G(\mathbf{J}_2)\,.$$

We remark that requirements (a),(b),(d),(e) are identical to the conditions formulated by Schultz and Kindlmann [15] for the special case

Tim Gerrits, Christian Rössl, and Holger Theisel are with the Visual Computing group at the University of Magdeburg, Germany. E-mail: {gerrits,roessl,theisel}@isg.cs.uni-magdeburg.de

Manuscript received 31 Mar. 2016; accepted 1 Aug. 2016. Date of publication 15 Aug. 2016; date of current version 23 Oct. 2016.
For information on obtaining reprints of this article, please send e-mail to: reprints@ieee.org, and reference the Digital Object Identifier below.
Digital Object Identifier no. 10.1109/TVCG.2016.2598998

of symmetric tensors, there called *symmetry preservation*, *invariance under scaling*, *disambiguity*, and *continuity*. They additionally demand a property called *invariance under eigenplane projections*. This property is not well-defined for general tensors as the eigenplanes may not be perpendicular or not even real at all. We replace their property by (c) which is stronger in some sense: it generalizes explicitly to the case of real but non-orthogonal eigenvectors, and it makes no assertion for the complex case.

3 Related Work

Most glyphs proposed in the literature are exclusively constructed for symmetric tensors. And among these, the majority is devoted to positive definite tensors. Rather than giving a complete review of these special cases, we mention two representative approaches: Kindlmann's superquadric tensor glyphs [8] for positive definite tensors, and Schultz' and Kindlmann's superquadric glyphs for general symmetric tensors [15]. We refer to the latter (and the references therein) for an in-depth discussion of the symmetric case. In a recent paper, Seltzer and Kindlmann [16] design glyphs for asymmetric second-order 2d tensors. We discuss and compare to this work in section 9.4.

There are few glyph techniques for non-symmetric tensors, that originate either from flow visualization (for visualizing the Jacobian of a flow field) or from mechanical engineering. A straightforward approach is to decompose a non-symmetric tensor $\mathbf{J}$ into a sum of the symmetric part $\frac{1}{2}(\mathbf{J}+\mathbf{J}^{\mathrm{T}})$ and the antisymmetric part $\frac{1}{2}(\mathbf{J}-\mathbf{J}^{\mathrm{T}})$. Then the symmetric part can be visualized by glyphs for symmetric tensors, and the antisymmetric part can be encoded and visualized as a vector. This way, however, the information about the eigenvalues and eigenvectors of the original tensor $\mathbf{J}$ is lost, and no direct encoding of this information is possible as required by (c).

In flow visualization, Globus et al. [6] propose to represent tensors with real eigenvalues by ellipsoids. Their approach does not consider complex eigenvalues, nor does it provide uniqueness thus lacking requirement (d). De Leeuw and van Wijk [3] propose a glyph that, among others, contains derived values from the Jacobian, where the eigenvalues of the Jacobian are not directly encoded, and thus lacking (c). Theisel et al. [19] propose a glyph that lacks uniqueness (c). Palke et al. [13] use glyphs for asymmetric tensors with complex eigenvalues. Their approach does not cover the complete space of 2d tensors, and they do not provide an extension to 3d. Zhang et al. [20] introduce the eigenvector manifold and visualize the 2d eigenvectors as line segments. This way, discontinuities can occur whenever eigenvectors are not well defined due to equal eigenvalues. Further approaches to visualizing non-symmetric tensors include [4, 11, 12]. None of these provides glyphs for the complete space of non-symmetric tensors.

In mechanical engineering, there exist several approaches to visualizing stress tensors [10]. Mohr's circles [2] visualize only eigenvalues, and are therefore lacking invariance to domain rotations (a). Haber glyphs [7] consist of an ellipsoid and a rod for the eigenvectors. The glyphs are continuous (lacking (e)) when the eigenvectors are not well-defined.

The following table gives an overview of existing work on 3d general tensor glyphs. Existing techniques are evaluated with respect to satisfying conditions (a)-(e) from section 2. In addition, the column (f) indicates if the technique is general, i.e., not restricted to symmetric tensors.

method / satisfies	(a)	(b)	(c)	(d)	(e)	(f)
Kindlmann and Schultz [8, 15]	✓	✓	✓	✓	✓	✗
tensor decomposition	✓	✓	✗	✓	✓	✓
Globus et al. [6]	✓	✓	✓	✗	✓	✓
de Leeuw and van Wijk [3]	✓	✓	✗	✗	✓	✓
Theisel et al. [19]	✓	✓	✓	✗	✗	✓
Mohr's circle [2]	✗	✗	✓	✗	✓	✓
Haber glyph [7]	✓	✓	✓	✗	✗	✓
this paper	✓	✓	✓	✓	✓	✓

We conclude this review with the statement that we are not aware of a glyph for general tensors – neither 2d nor 3d – that fulfills all conditions (a)-(e).

4 Preliminaries and Notation

Prior to the construction of glyphs we review some auxiliary concepts and notation. Given is a tensor $\mathbf{J} \in \mathbb{R}^{n\times n}$ for $n = 2, 3$.

Factorizations. We make use of the following matrix factorizations (see, e.g., [17]). The *spectral decomposition* $\mathbf{J} = \mathbf{X}\Lambda\mathbf{X}^{-1}$ yields the eigenvectors $\mathbf{X}_{.i}$ as columns of $\mathbf{X}$ and the eigenvalues λ_i as entries of the diagonal matrix Λ. For symmetric $\mathbf{J} = \mathbf{J}^{\mathrm{T}}$ the eigenvalues λ_i are real, and eigenvectors are orthogonal, i.e., $\mathbf{X}^{-1} = \mathbf{X}^{\mathrm{T}}$. For non-symmetric tensors, the eigenvectors are no longer orthogonal, and eigenvalues and eigenvectors may no longer be real.
The *singular value decomposition (SVD)* $\mathbf{J} = \mathbf{U}\Sigma\mathbf{V}^{\mathrm{T}}$ yields the orthogonal matrices $\mathbf{U}, \mathbf{V}$ and the diagonal matrix Σ with real, non-negative entries σ_i, the singular values $\sigma_1 \geq \sigma_2 \geq \ldots$

The SVD can be used to construct the *polar decomposition*

$$\mathbf{J} = (\mathbf{U}\mathbf{V}^{\mathrm{T}})(\mathbf{V}\Sigma\mathbf{V}^{\mathrm{T}}) = \mathbf{Q}\mathbf{H},$$

which factors an isometry represented as the orthogonal matrix $\mathbf{Q}$ and scaling/shear as the symmetric, positive definite matrix $\mathbf{H}$ with $\lambda_i(\mathbf{H}) = \sigma_i(\mathbf{J})$. $\mathbf{Q}$ is a rotation matrix if $\det(\mathbf{Q}) = +1$. In $\mathbb{R}^2$, a rotation matrix $\mathbf{Q}$ can be parametrized by an angle γ, which is given by $\tan\gamma = \mathbf{Q}_{21}/\mathbf{Q}_{11}$.

Isometry invariant tensors. Assume the tensor $\mathbf{J}$ represents the Jacobian matrix of a w.l.o.g. linear vector field. Then for any domain point $\mathbf{x}$ the vector $\mathbf{v} = \mathbf{v}(\mathbf{x})$ is given as $\mathbf{v} = \mathbf{J}\mathbf{x}$. For a generalization, we may interpret the restriction to a linear vector field as a local analysis using a Taylor expansion.

Given is an orthogonal matrix $\mathbf{Q}$ that represents an isometric map, e.g., a rotation. Then an isometric map of the domain $\mathbf{Q}^{\mathrm{T}}\mathbf{x}$ determines an isometry of the vector field. We consider

$$\mathbf{v}' = \mathbf{v}'(\mathbf{x}) = \mathbf{Q}\,\mathbf{v}(\mathbf{Q}^{\mathrm{T}}\mathbf{x}) = \mathbf{Q}\,\mathbf{J}\,\mathbf{Q}^{\mathrm{T}}\mathbf{x} = \mathbf{J}'\mathbf{x},$$

and define $\mathbf{J}' = \mathbf{Q}\,\mathbf{J}\,\mathbf{Q}^{\mathrm{T}}$ as a (domain) *isometry* of the tensor $\mathbf{J}$. We call a tensor *invariant* to isometry iff $\mathbf{J}' = \mathbf{J}$.

(γ, r)-parametrization of tensors. Theisel and Weinkauf [18] parameterize a subspace of 2d tensors $\mathbf{T}$ using two scalar parameters γ and r such that using polar decomposition

$$\mathbf{T} = \mathbf{Q}\mathbf{H} = \begin{pmatrix}\cos\gamma & -\sin\gamma \\ \sin\gamma & \cos\gamma\end{pmatrix}\begin{pmatrix}1 & \\ & \sigma_2\end{pmatrix},$$

i.e., the spectral norm of $\mathbf{T}$ is *constrained* to $||\mathbf{T}||_2 = \sigma_1(\mathbf{T}) = 1$, and there is no orthogonal transform in $\mathbf{H}$ (i.e., the right singular vectors $\mathbf{V} = \mathbf{I}$), which can be interpreted as "factoring out" domain rotations. The parameter $\gamma \in [0, 2\pi)$ determines rotation, and the parameter $r \in [0, 1]$ determines $\mathbf{T}$'s smaller singular value $\sigma_2 = \frac{1-2\sqrt{(1-r)r}}{2r-1} \in [-1, 1]$. Here, σ_2 is exceptionally equipped with a sign, which expresses the sign of the determinant $\mathrm{sgn}(\sigma_2) = \mathrm{sgn}(\det(\mathbf{T}))$.

This subspace suffices to study and describe all classes of 2d tensors. And conversely, *arbitrary* tensors $\mathbf{J}$ can be mapped to the (γ, r)-plane using polar decomposition and $r = \frac{1}{2} + \det(\mathbf{J})/||\mathbf{J}||_F^2 = \frac{1}{2} + \mathrm{sgn}(\det(\mathbf{J}))\,\frac{\sigma_1\sigma_2}{\sigma_1^2+\sigma_2^2}$, where $||\mathbf{J}||_F^2$ denotes the Frobenius norm.

Theisel and Weinkauf use the (γ, r)-parametrization for designing a distance metric on tensors. We utilize the following properties throughout the paper: Given is a tensor $\mathbf{J}$ and its mapping to the (γ, r)-plane. Then the following statements hold [18].

(i) Let $r^\star = \frac{1}{1+\sin^2\gamma}$. Then $r^\star \geq \frac{1}{2}$, and

$$\mathbf{J} \text{ has eigenvalues } \begin{cases} \lambda_1 \neq \lambda_2 \in \mathbb{R} & \text{for } r < r^\star \\ \lambda_1 = \lambda_2 \in \mathbb{R} & \text{for } r = r^\star \\ \lambda_1 = \overline{\lambda_2} \in \mathbb{C} & \text{else} \end{cases}.$$

(ii) $$\det(\mathbf{J}) = \lambda_1\lambda_2 \begin{cases} < 0 & \text{for } 0 \leq r < \frac{1}{2} \\ = 0 & \text{for } r = \frac{1}{2} \\ > 0 & \text{else} \end{cases}.$$

Notation. In the remainder of the paper, $\mathbf{U},\mathbf{V},\mathbf{Q}$ denote orthogonal matrices – $\mathbf{U},\mathbf{V}$ are singular vectors from SVD, and $\mathbf{Q}$ denotes a general an isometric transform, the factor from polar decomposition or a 2d rotation matrix $\mathbf{Q}(\gamma)$ – and Λ,Σ are diagonal matrices with eigenvalues λ_i and non-negative singular values σ_i as usual in descending order. $\mathbf{X}$ denotes a matrix that has unit-length eigenvectors as columns, and we write $\mathbf{X}_{.i}$ for the i-th column. The symbols γ and r refer to the (γ,r)-parametrization of 2d tensors. Whenever the context is clear, we omit the explicit reference to the tensor and write, e.g., λ_i or γ instead of $\lambda_i(\mathbf{J})$ or $\gamma(\mathbf{J})$.

5 Glyphs for 2D Tensors

This section presents the construction of glyphs for 2d tensors that meets all requirements (a)-(e) postulated in section 2. For the sake of a concise and focused presentation, some details (e.g., geometric primitives) are reviewed in the Appendix.

5.1 Preliminary Consideration

We start with a general observation that strongly influences the glyph design:.

Proposition 5.1. *It is impossible to use only shape for defining a glyph that satisfies conditions (a)-(e). At least one more continuous value has to be encoded in a channel different from shape.*

Proof. Consider tensors $\mathbf{J}$ that are constant under domain rotation, i.e.,

$$\mathbf{Q}\,\mathbf{J}\,\mathbf{Q}^{\mathrm{T}} \;=\; \mathbf{J} \tag{3}$$

for any rotation matrix $\mathbf{Q}(\gamma)$. Choose two such tensors of equal scale (norm) $\mathbf{J}_1 = \left[\begin{smallmatrix}1&0\\0&1\end{smallmatrix}\right]$, $\mathbf{J}_2 = \left[\begin{smallmatrix}0&-1\\1&0\end{smallmatrix}\right]$. Then (1) and (3) require that $\mathbf{Q}G(\mathbf{J}_1) = G(\mathbf{J}_1)$ and $\mathbf{Q}G(\mathbf{J}_2) = G(\mathbf{J}_2)$, i.e., an arbitrary rotation of the glyph gives the same glyph. The only shape that fulfills this requirement is the circle. Hence, both $\mathbf{J}_1$ and $\mathbf{J}_2$ must be encoded as the same circle. If glyphs are only determined by shape, this violates the requirement for uniqueness (d). In general, every tensor of the form $\mathbf{J} = \mathbf{Q}(\gamma)$ is constant under domain rotation and must therefore be mapped to the circle. Thus, we need at least one additional continuous channel to encode the angle γ in the glyph: We use color. □

In the following, we separate the construction into designing shape and mapping color.

5.2 Shape

Given is a tensor $\mathbf{J} \in \mathbb{R}^{2\times 2}$ with eigenvalues $\lambda_{1,2}$. The basic geometric primitive for the construction of the shape of the associated glyph is the *characteristic ellipse* of $\mathbf{J}$ that we define as the point set that satisfies

$$\mathbf{x}^{\mathrm{T}}(\mathbf{J}\mathbf{J}^{\mathrm{T}})^{-1}\mathbf{x} \;=\; 1\;. \tag{4}$$

This implicit curve is an ellipse that interpolates for $\lambda_{1,2} \in \mathbb{R}$ the eigenvectors scaled by eigenvalues, i.e., the columns of $\pm\mathbf{X}\Lambda$. Note that in general, the eigenvectors $\mathbf{X}$ are *not* orthogonal. For *complex* eigenvalues, the orthogonal axes of the ellipse are spanned by the left singular vectors $\mathbf{U}$. The Appendix gives a proof of these properties.

We parameterize the implicitly defined characteristic ellipse as a piecewise rational quadratic Bézier curve [5], where each piece is an arc with the the scaled eigenvectors (or left singular vectors if $\lambda_i \in \mathbb{C}$) as end points. Each piece is defined by three control points $\mathbf{b}_i$ and weights w_i. Due to end point interpolation, $\mathbf{b}_0, \mathbf{b}_2$ are given by the scaled eigenvectors with standard weights $w_0 = w_2 = 1$. The center control point is

$$\mathbf{b}_1 \;=\; \omega\,(\mathbf{b}_0+\mathbf{b}_2) \quad \text{with weight } w_1 \;=\; \cos\alpha/2\;,$$

with

$$\omega \;=\; \frac{1}{1+\cos\alpha} \tag{5}$$

where α is the angle enclosed by $\mathbf{b}_0, \mathbf{0}, \mathbf{b}_2$ (or two eigenvectors, respectively). This results in two rational pieces for the smaller and larger enclosed angle, and the remaining two pieces can be determined from symmetry. Figure 2a shows an example, and the Appendix gives a construction of the parametrization.

We consider the mapping of $\mathbf{J}$ into the (γ,r)-plane, and use γ and r to distinguish different cases based on properties (i) and (ii). Each case determines a *modification* of the characteristic ellipse, and each modification is defined in a way that guarantees requirements (a)-(d) and in particular (e), the continuous transition between the different cases. We emphasize this by explicitly reviewing the transitions as special cases. All modifications are described for one rational piece $(\mathbf{b}_i, w_i)$, $i = 0,1,2$, with $\alpha = \angle(\mathbf{b}_0, \mathbf{0}, \mathbf{b}_2)$. The same modification is applied equally to all pieces. Let $r^\star = \frac{1}{1+\sin^2\gamma}$.

Case $0 \le r < \frac{1}{2}$. $\mathbf{J}$ has real eigenvalues and a negative determinant $\lambda_1\lambda_2 < 0$. The glyph for this "saddle" configuration should be a *concave* shape that conveys the directions and magnitude of eigenvectors and eigenvalues, which can be interpreted as "inflow" and "outflow" if the tensor is a Jacobian matrix of a vector field. Each arc of the characteristic ellipse is modified such that the center control point is moved to $\frac{1}{2}\,|\cos\alpha|\,(\mathbf{b}_0+\mathbf{b}_2)$. This yields a concave shape as $\mathbf{b}_1$ is closer to the origin $\mathbf{0}$ than $\frac{1}{2}(\mathbf{b}_0+\mathbf{b}_2)$. Figure 2b shows an example.

Case $r = \frac{1}{2}$. At this transition, $\mathrm{rank}(\mathbf{J}) = 1$, and one of the two real eigenvalues vanishes, i.e., $\lambda_1\lambda_2 = 0$. As a consequence, the characteristic ellipse "degenerates" to a line segment. The behavior is continuous as for $h \to 0$, both $r = \frac{1}{2} \pm h$ result in the same glyph.

Case $\frac{1}{2} < r < r^\star$. This is probably the simplest case of a positive definite ($\lambda_{1,2} > 0$) or negative definite ($\lambda_{1,2} < 0$) tensor $\mathbf{J}$. The glyph should be *convex* and clearly indicate the directions and magnitude of eigenvectors and eigenvalues. We modify the smooth characteristic ellipse such that there are sharp bends in these directions, i.e., the curve should be only C^0-continuous at the end points $\pm\mathbf{X}\Lambda$ of the elliptic arcs. Note that $\mathbf{X}$ is orthogonal only for symmetric $\mathbf{J}$. For general tensors, the indicated directions do *not* coincide with the principal axes of the characteristic ellipse.

For each arc, we move the center control point towards $\frac{1}{2}(\mathbf{b}_0+\mathbf{b}_2)$ as follows: Define the ratio $\tau = \lambda_1/\lambda_2$ of eigenvalues and $\tau^\star = \min\{\tau, 1/\tau\} \in [0,1]$, and let

$$\omega^\star \;=\; (1-|\sin\gamma|)\,\left((1-\tau^\star)\,\tfrac{1}{2} + \tau^\star\,\omega\right) + |\sin\gamma|\;\omega\;. \tag{6}$$

The new position of the center control point is $\mathbf{b}_1 = \omega^\star(\mathbf{b}_0+\mathbf{b}_2)$. In order to ensure that sharp bends develop more rapidly near the transitions $r = \frac{1}{2}$ and $r = r^\star$, we suggest to apply an additional transfer function and to replace $\tau^\star$ in the above formula by $f(\tau^\star)$ with $f(t) = 4\,(t-\frac{1}{2})^3 + \frac{1}{2}$. Figure 2c shows an example.

The amount of "sharpening" is maximal at the transition $r = \frac{1}{2}$ – think of the "degenerated stick" as a "diamond" – and it gradually fades out towards the smooth characteristic ellipse as $r \to r^\star$ and the smaller angle enclosed by two eigenvectors vanishes.

Case $r = r^\star$. At this transition, the eigenvalues are equal $\lambda_1 = \lambda_2$, and the eigenvectors are parallel, i.e., the smaller of the enclosed angles is zero. The shape of the glyph is the characteristic ellipse *without modification*.

Case $r^\star < r \le 1$. $\mathbf{J}$ has complex eigenvalues $\lambda_1 = \overline{\lambda_2}$. The principal axes of the characteristic ellipse are spanned by the left singular vectors of $\mathbf{J}$. *No modification* is applied.

Case $r = 1$. In the limit, $\mathbf{J}$ is a rotation matrix $\mathbf{Q}(\gamma)$ as with $r = 1$ its singular values must be equal $\sigma_1 = \sigma_2$. This follows from the definition of the (γ,r)-parametrization using the constrained-norm tensor $\mathbf{T}$ with $||\mathbf{T}||_2 = \sigma_1(\mathbf{T}) = 1$: with $r = 1$ we have also $\sigma_2(\mathbf{T}) = 1$. Then $\mathbf{J}$ is invariant to domain rotation, and also the glyph must be invariant to rotation. The shape of the glyph is just the characteristic ellipse, which is a circle for $\sigma_1 = \sigma_2$. Figure 6 shows different shapes in the (γ,r)-plane.

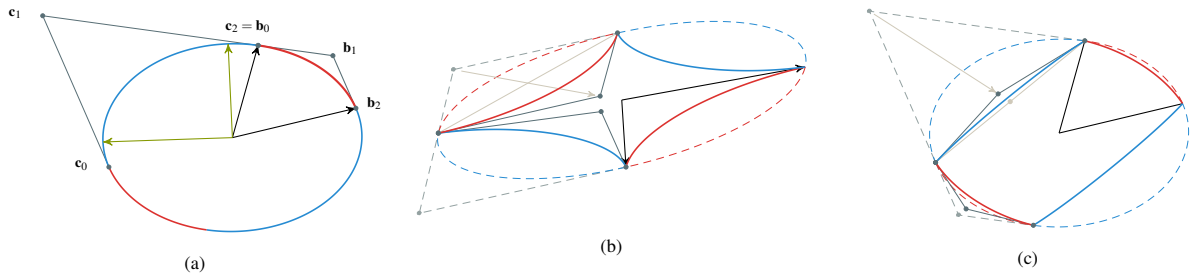

Fig. 2: (a) Characteristic ellipse of a non-symmetric tensor with real eigenvalues. The black arrows denote the eigenvectors scaled by the eigenvalues ($\mathbf{X}\Lambda$), and the green arrows show the orthogonal left singular vectors scaled by singular values ($\mathbf{U}\Sigma$). The four arcs are parametrized as rational quadratic Bézier curves shown in red and blue. The control polygons $\mathbf{b}_i, \mathbf{c}_i$ are shown for two arcs (in gray). Joining rational pieces smoothly at $\mathbf{b}_0$ requires that $\mathbf{c}_1, \mathbf{c}_2 = \mathbf{b}_0$, and $\mathbf{b}_1$ are colinear. (b) For a saddle configuration, the center control points, e.g., $\mathbf{b}_1$ of the original characteristic ellipse configuration (dashed) are moved "beyond" $\frac{1}{2}(\mathbf{b}_0 + \mathbf{b}_2)$ towards the origin to obtain a concave shape (solid). (c) For a positive definite tensor, we introduce sharp bends to indicate the directions of the eigenvectors. The center control points are moved closer towards $\frac{1}{2}(\mathbf{b}_0 + \mathbf{b}_2)$.

5.3 Color

We use color to encode the angle γ. For $r \geq \frac{1}{2}$, each glyph is filled with a single, "flat" color.

Any continuous color map of the circle is possible. We use the color map shown in figure 3 that maps positive and negative definite ($\gamma = 0$ and $\gamma = \pi$) tensors to red and blue tones, and 90 degree rotations ($\gamma = \pi/2$ and $\gamma = 3\pi/2$) to yellow and green tones, respectively.

The "saddle" case $r < \frac{1}{2}$ is treated differently, because we want to distinguish the directions of inflow and outflow and thus use two colors. First, we have to make sure that one color gives a continuous transition along the circle $r = 1/2$ in the (γ, r)-space. Let $\lambda_1 \leq 0 \leq \lambda_2$, and the corresponding eigenvectors $\mathbf{X}_{\cdot 1}$ and $\mathbf{X}_{\cdot 2}$ oriented such that $\det(\mathbf{X}) < 0$, further let $\alpha \in [0, \pi]$ be the angle enclosed by $\mathbf{X}_{\cdot 1}$ and $\mathbf{X}_{\cdot 2}$. Then we get two γ-values

$$\gamma_1 = \frac{\pi}{2} + \alpha \quad \text{and} \quad \gamma_2 = \frac{\pi}{2} - \alpha \,,$$

that are color-coded as described above. The inner circles in figure 3 show the two colors for the respective points in (γ, r)-space.

In addition, a partition of the glyph's geometry is required. Let $\mathbf{f}_i(t) : [0,1] \to \mathbb{R}^2$, $i = 0, \ldots, 3$, denote the four rational pieces that define the boundary of the glyph. With a circular shift of the "global" parametrization by $1/2$ we obtain

$$\mathbf{g}_i(t) = \begin{cases} \mathbf{f}_i(t + 1/2) & \text{for } t \leq 1/2 \\ \mathbf{f}_{i+1 \bmod 4}(t - 1/2) & \text{for } t > 1/2 \end{cases}, \quad i = 0, \ldots, 3 \,,$$

such that each image of $\mathbf{g}_i(t) : [0,1] \to \mathbb{R}^2$ consists of two half-arcs that indicate the direction of an eigenvector. This partitions the glyph symmetrically into four patches. Figure 6 shows different shapes and colors in the (γ, r)-plane.

6 Glyphs for 3D Tensors

We utilize the 2d construction and in particular the (γ, r) parametrization as much as possible the 3d setting for general tensors $\mathbf{J} \in \mathbb{R}^{3\times 3}$. This leads to two cases depending on the configuration of eigenvectors and eigenvalues: In the first case there is one distinct pair of eigenvalues either having the opposite sign to the third one or being complex conjugates. In this case, the distinct pair of eigenvectors (for real eigenvalues) or left singular vectors (for complex eigenvalues) span a uniquely defined *base plane*. In the second case, no distinctive eigenvectors exist because all three eigenvalues are real and positive (or all three are real and negative). For both cases, we discuss first shape and then color of the glyph.

6.1 Case 1: A well-defined base plane exists.

Shape. A well-defined base plane exists, if either all eigenvalues are real and one differs in sign, or if two eigenvalues are complex conjugates. In the first case ("saddle"), the plane is spanned by the eigenvectors corresponding to the two eigenvalues with same sign. In the second case ("swirling"), the plane is spanned by the left singular vectors. It is straightforward, to extend the condition to eigenvalues equal to zero, which require the usual "numerical caution" when dealing with near zero values.

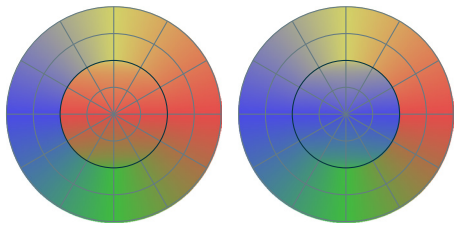

Fig. 3: The glyph's color is determined by the angle γ. The figure shows the color map used in this paper as the outer band ($r \geq 1/2$) of the color wheel with superimposed polar coordinate system (γ, r). Darker circles indicate $r = 1/2$. The color is constant for $1/2 \leq r \leq 1$. Two colors are required for saddles ($r < 1/2$) to indicate "inflow" and "outflow" directions. We use complementary colors shown in the inner circles that also depend on the angle enclosed by the (real) eigenvectors.

We construct the shape from eight triangular patches. One of them is shown in figure 4a. Suppose that $\mathbf{x}_1$ and $\mathbf{x}_2$ are the scaled eigenvectors spanning the base plane, and $\mathbf{x}_3$ is the remaining scaled eigenvector. Then the intersection of the desired patch with the base plane is exactly the solution of the 2d glyph in the base plane. Furthermore, we use the information from the base plane as well as the ratio between the associated eigenvalues and the remaining eigenvalue to determine the shape outside the base plane. We describe the patch as a rational bi-quadratic patch $\mathbf{f}(u, v)$ with a degeneracy, i.e., an undefined normal, at $\mathbf{x}_3$, where the parameters w_{12}, μ_{12} and ν_{12} (see figure 4b) are determined as follows. w_{12} and μ_{12} are chosen such that we get the 2d glyph is in the base plane: μ_{12} is obtained similarly to (5), and w_{12} is obtained similarly to (6). The remaining ν_{12} determines the global convexity/concavity of the shape and is chosen as

$$\lambda_{12} = \frac{\lambda_1 + \lambda_2}{2}, \quad \nu_{12} = \frac{1}{2} + \frac{1}{2}\,\mathrm{sgn}(\lambda_{12}\lambda_3)\left(|\cos\gamma|\,\frac{|2\lambda_{12}\lambda_3|}{\lambda_{12}^2 + \lambda_3^2}\right)^n$$

where γ is from the (γ, r) parametrization of the projection of $\mathbf{J}$ into the base plane, and the exponent n controls "sharpness" of the shape near discontinuities. This patch construction is repeated eight times for each combination of $\pm\mathbf{x}_i$ as patch corners to obtain the entire shape. The resulting patches have the following properties.

- $\mathbf{f}_u(0,v) = h(v)\mathbf{f}_u(0,0)$ for a certain function $h(v)$. This means that the partial derivative of $\mathbf{f}$ w.r.t. u does not change direction along the boundary curve from $\mathbf{x}_1$ to $\mathbf{x}_3$. (A similar statement holds for $\mathbf{f}_u(1,v)$.) As a consequence, in case of the characteristic ellipse as base shape, adjacent patches are G^1-*continuous* along the junction curves that are not in the base plane.

- If $\mathbf{x}_1, \mathbf{x}_2, \mathbf{x}_3$ build an orthonormal system, $\mathbf{f}(u,v)$ is the octant of a sphere (see [14]).

Details of the patch construction are reviewed in the Appendix.

Color. The glyph consists of the following colors: Close to the base plane, we color code the γ value of the 2d case in the projection into the base plane. Note that depending on the side of the base plane, this requires two different colors. If from one side the value γ is encoded, the view from the other side must encode $-\gamma$. For the coloring of the regions close to $\mathbf{x}_3$ a binary choice is sufficient: red for $\lambda_3 > 0$, blue else. It remains to define at what v-value the "hard" transition between the two colors takes place. We choose $v = \frac{\sigma_1}{\sigma_1+\lambda_3}$, where $\sigma_1 = \sigma_1(\mathbf{J}_P) = ||\mathbf{J}_P||_2$ is the spectral norm of the projection of $\mathbf{J}$ into the base plane. This makes sure that for $\lambda_3 \to 0$, the color of the whole 3d shape converges to the color of the 2d glyph in the base plane.

6.2 Case 2: There is no unique base plane.

Shape. In this case, all pairs of eigenvectors can be chosen equally to span a base plane. This means that depending on the particular choice, we have three different patches for each octant of the shape. We propose to blend patches using a weighted average. For this, two problems have to be solved: (1.) The three patches are given in different parametrization, which prohibits a direct blending. (2.) The blend weights must be chosen to ensure a smooth transition of the shape between case 1 and case 2. To solve the first problem, we apply a non-standard reparametrization of the patch from u,v-coordinates to barycentric coordinates $\beta_1+\beta_2+\beta_3 = 1$, which is detailed in the Appendix.

To address the second problem, the blend weights for patch evaluation are chosen as

$$\begin{aligned} W_1 &= |(\lambda_3-\lambda_1)(\lambda_3-\lambda_2)\lambda_1\lambda_2| \\ W_2 &= |(\lambda_1-\lambda_2)(\lambda_1-\lambda_3)\lambda_2\lambda_3| \\ W_3 &= |(\lambda_2-\lambda_3)(\lambda_2-\lambda_1)\lambda_3\lambda_1| \end{aligned} \tag{7}$$

This ensures that if, e.g., λ_1 and λ_2 get close to each other, W_1 and W_2 get close to 0, meaning that we have the desired smooth transition between case 1 and case 2. The same desired transition takes place for $\lambda_3 \to 0$. If all eigenvalues are identical, the patches are also identical, and all weights would equally evaluate to zero and would lead to a degenerate patch. In this case all weights are set to an equal, nonzero value.

Color. For color, we use the same weighted average as for shape. For every barycentric coordinate $\beta_1, \beta_2, \beta_3$ we have a γ value for each patch (either the γ-value of the base plane, or $\gamma = 0$ or $\gamma = \pi$ towards the patch corner away from the base plane). The three γ-values are averaged by the same blend weights W_1, W_2, W_3. Note that this way, one final patch can consist of up to eight different colors. However, in practice, they can hardly be distinguished: all of them are rather red (for outflow) or rather blue (for inflow). This is desired because in this case all relevant information for uniqueness lies in the shape. We have to apply this seemingly complicated color mapping to ensure continuity between case 1 and case 2.

6.3 Eigensticks

Our 3d construction so far does not ensure uniqueness for the case $\text{rank}(\mathbf{J}) = 2$. In this case, no information about the direction of the eigenvector corresponding to the zero eigenvalue is encoded in the glyph. This can be fixed by additionally rendering eigensticks, i.e., carefully scaled real eigenvectors of $\mathbf{J}$ as

$$\begin{aligned} &\pm(\lambda_1-\lambda_2)(\lambda_1-\lambda_3)\mathbf{X}_{\cdot 1}\,, \\ &\pm(\lambda_2-\lambda_1)(\lambda_2-\lambda_3)\mathbf{X}_{\cdot 2}\,, \\ &\pm(\lambda_3-\lambda_1)(\lambda_3-\lambda_2)\mathbf{X}_{\cdot 3}\,, \end{aligned}$$

with $\mathbf{X}_{\cdot i}$ denoting the i-th eigenvector. In most cases, eigensticks are rendered *inside* the shape and therefore not visible. Only in the case of flat shapes, i.e., there is one rather small eigenvalue, they become visible. Figure 5 shows an example. Note that eigensticks also fulfill the continuity condition for coinciding eigenvalues the corresponding eigensticks converge to the zero vector.

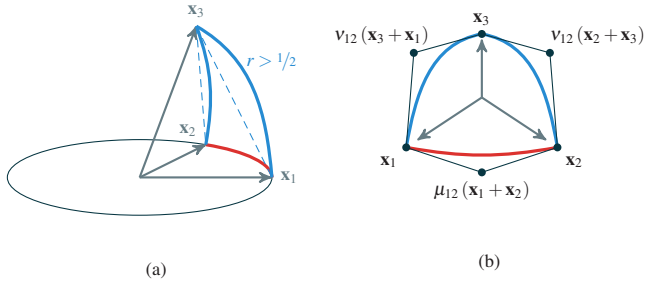

Fig. 4: (a) If a base plane exists, it defines an ellipse, and every rational piece (red) defines a surface patch together with the two other arcs (blue and gray), which use a standard weight $\sqrt{2}/2$. (b) Similar to 2d, the control points are determined as linear combinations of scaled eigenvectors $\mathbf{x}_i$. Note that without well-defined base plane, all three possible patches are evaluated and "blended".

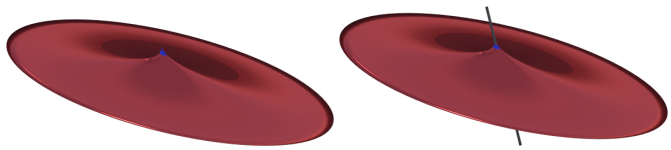

Fig. 5: Flat-shaped glyph without (left) and with eigenstick (right).

7 Results

Figure 6 samples the (γ, r)-plane and show the corresponding glyphs. Figure 7 shows (scaled) glyphs that visualize the Jacobian matrix of a 2d slice of the flow behind a square cylinder. The underlying flow field is visualized by a LIC texture with the superimposed glyphs. The glyphs vary significantly in scale, and there are regions of rapid transition between different glyphs. Two closeups zoom into interesting regions.

Figure 1 shows a selection of different glyphs for 3d tensors together with the eigenvalues in the complex plane. More examples are given in figure 8 which includes two cases with one of the three real eigenvectors getting close to zero: the corresponding glyphs have a flat shape (not seen from the chosen perspective), and the eigensticks become visible and convey the direction of the eigenvector associated with the near-zero eigenvalue.

Figure 9 shows 3d glyphs in the Jacobian field of a flow that stems from a simulation of a Rayleigh-Bénard convection. The underlying flow field is illustrated with few illuminated streamlines.

3d glyphs that are close to rank 2 appear flat, which makes it difficult to recognize the direction of the eigenvector corresponding to the near-zero eigenvalue. Eigensticks as described in the previous section 6.3 remedy this deficiency. Figure 5 explicitly compares the same glyph with and without rendering an eigenstick that emphasizes the direction of the eigenvector.

8 How to read the glyphs

The glyphs proposed in this paper encode a significant amount of information. Moreover, the requirements (a)-(e) postulated in section 2

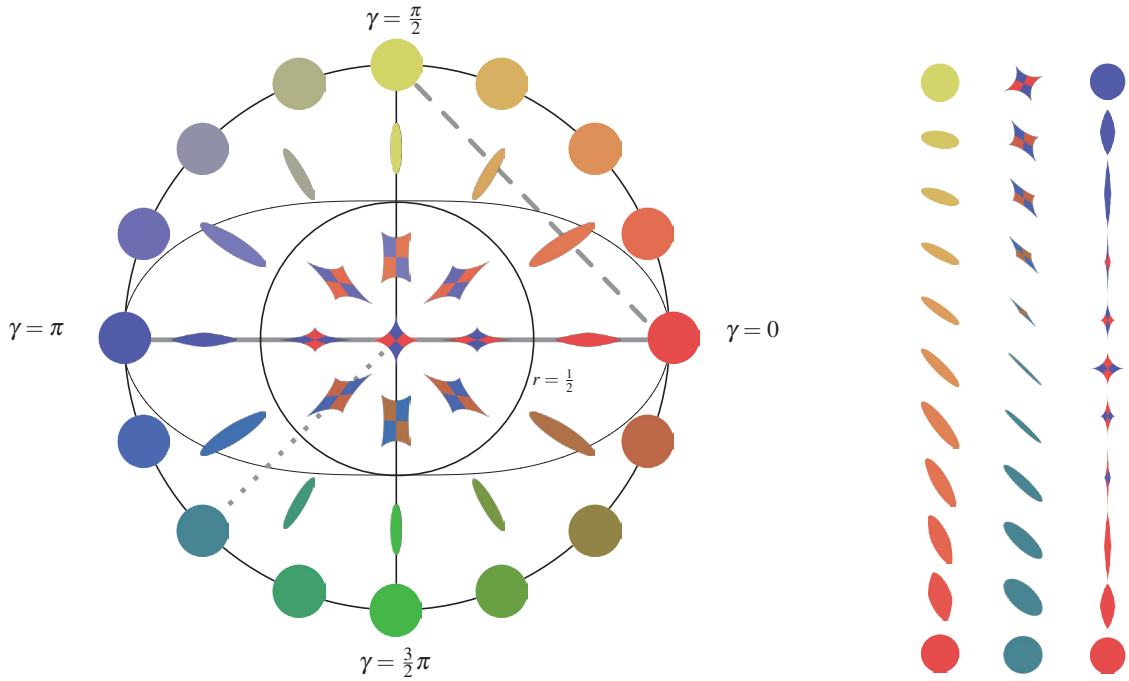

Fig. 6: Sampling glyphs in the (γ, r)-plane. The circles on the left figure indicate $r = 1/2$ (zero determinant on the transition between saddle and definite) and $r = 1$ (equal eigenvalues), and the oval shape is the curve $r = r^\star$ (equal eigenvectors and eigenvalues on the transition between real and complex). The right figure shows sampled glyphs corresponding to the line segments. Left column: dashed line $(\gamma, r) = (1-t)\,(0,1) + t\,(\pi/2, 1)$; center column: dotted line $\gamma = 5\pi/4$; right column: solid line $\gamma \in \{0, \pi\}$.

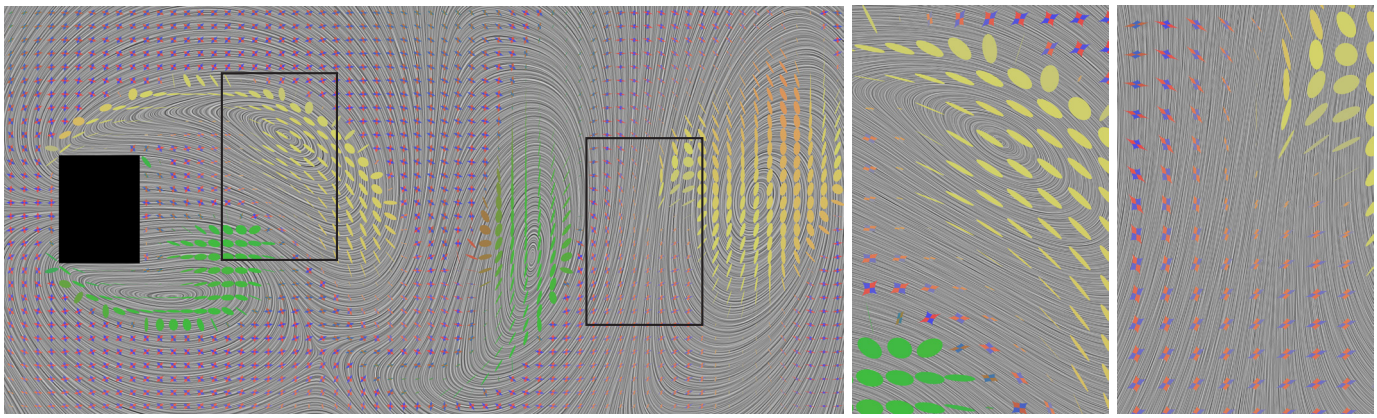

Fig. 7: Glyphs visualizing the Jacobian matrix of the flow around a square cylinder with two closeups (rectangles). The underlying LIC image visualizes the flow.

constrain design choices and make the appearance of glyphs different from previous works. In this section, we show that despite this fact the new glyphs are easy to use by providing a few simple rules on how to read the proposed glyphs.

Shape. *Convex* shapes indicate that all real eigenvalues have the same sign or positive determinant, while *concave* shapes indicate different sign of eigenvalues.

An *ellipse* in 2d indicates that there are no unique real eigenvectors, for either case of complex or identical real eigenvalues.

An *ellipsoid*, i.e., a smooth shape without discontinuities, in 3d is only possible as a sphere, i.e., for three identical real eigenvalues (see figure 1, left). Shape discontinuities at *sharp corners* in 2d and in addition *sharp edges* in 3d (see figure 1, 2nd left) encode the direction of real eigenvectors for symmetric and asymmetric tensors without rotation.

Color. *Red* indicates positive real eigenvalues, i.e., an outflow, and *blue* indicates negative real eigenvalues, i.e., an inflow.

Yellow indicates counterclockwise swirling, and *green* indicates clockwise swirling.

9 Discussion

In this section we verify that the proposed glyphs fulfill the requirements (a)-(e) postulated in section 2, and we discuss our various design decisions.

9.1 Fulfillment of requirements

(a) *Invariance under isometric domain transformations*. The property holds because all constructions are based on scaled eigenvectors $\mathbf{X}\Lambda$ of $\mathbf{J}$ (in the real case) or on scaled left singular vectors $\mathbf{U}\Sigma$ (in the complex case) and their linear combinations for determining control points. Both, $\mathbf{X}$ and $\mathbf{U}$ are invariant under isometric domain transformations $\mathbf{Q}$, as for $\mathbf{J} = \mathbf{X}\Lambda\mathbf{X}^{\mathrm{T}} = \mathbf{U}\Sigma\mathbf{V}^{\mathrm{T}}$, $\mathbf{QJQ}^{\mathrm{T}}$ has eigenvectors

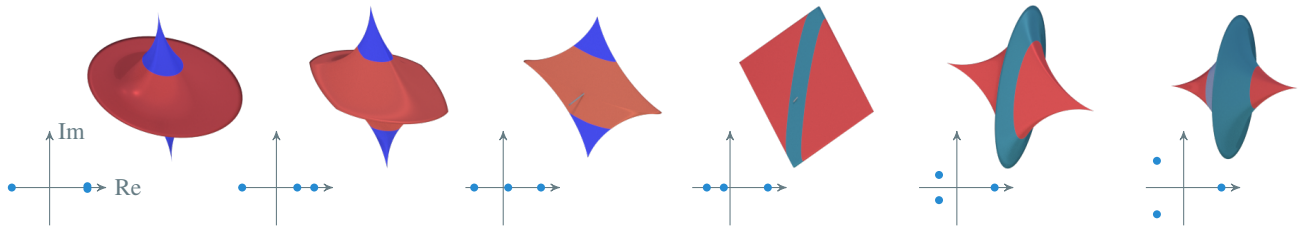

Fig. 8: Selection of glyphs for 3d tensors with their eigenvalues plotted in the complex plane. Note that the two center glyphs feature visible eigensticks due to one of the three eigenvalue getting close to zero.

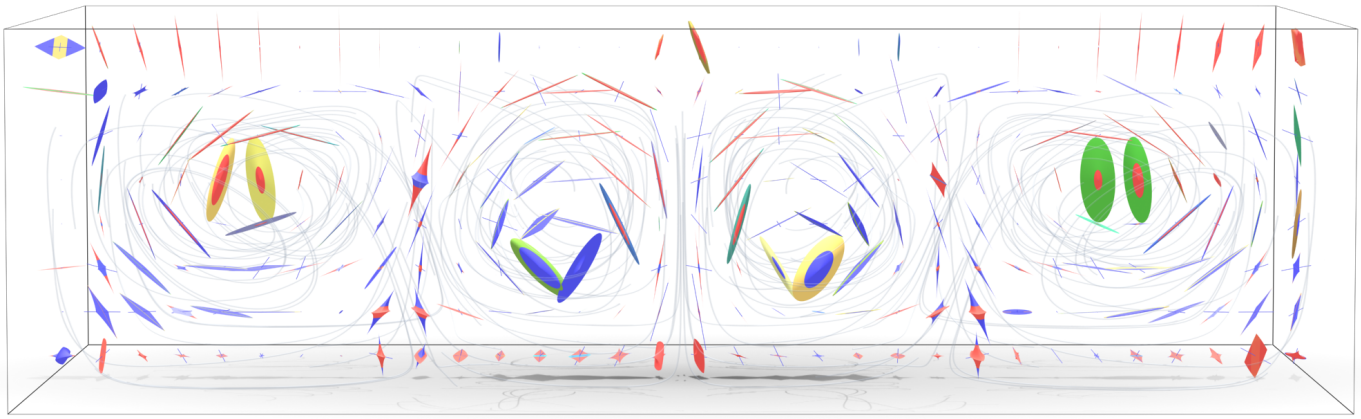

Fig. 9: The glyphs depict the Jacobian matrices of a flow field from the simulation of a Rayleigh-Bénard convection. The illuminated streamlines give an impression of the flow.

QX and singular vectors **QU** and **QV** regardless of the dimension.

(b) *Scaling Invariance* follows directly from the construction.

(c) *Direct encoding of real eigenvalues and eigenvectors.* This follows also directly from the construction as all scaled eigenvectors appear visually as points or curves of C^0 continuity, i.e., as sharp bends due to discontinuities of the glyph's tangent field.

(d) *Uniqueness.* In 2d, it is sufficient to show that for every point in the (γ, r) phase space there is a different glyph, i.e., two such glyphs are not identical after rotation. For real eigenvalues, this follows directly from (c) because a tensor is uniquely defined by its eigenvalues and eigenvectors. In the complex case, the glyph is the characteristic ellipse. Since its aspect ratio uniquely encodes r and its color uniquely encodes γ, the glyph must be unique. Note that uniqueness also holds for 2d tensors of rank 1: they are encoded as sticks of a unique color that depends on γ.

In 3d, in the case of a well-defined base plane and non-zero third eigenvalue, the property follows from the 2d case in the base plane and the unique visibility of the third eigenvector. In the case of three all positive (or all negative) real eigenvalues, all eigenvectors are visible and the property follows from (c). With this, *weak* uniqueness in 3d is shown.

A special case in 3d is $\text{rank}(\mathbf{J}) = 2$, then the glyph is a 2d figure in the plane of the non-zero eigenvectors. In this case, the direction of the eigenvector corresponding to the 0 eigenvalue is not encoded in the glyph's shape and color. Hence we do not have uniqueness. The solution is the optional addition of the eigensticks (section 6.3) that ensures the uniqueness of this case.

Another special case in 3d is $\text{rank}(\mathbf{J}) = 1$, which gives a stick as glyph. To ensure uniqueness in this case, we additionally have to encode the eigenplane of the zero eigenvalues. Since the space of all possible eigenplanes is two-parametric, it cannot be encoded solely by color, hence, the glyph is not unique in this case. We decided not to introduce additional features to remedy this for the sake of avoiding further visual clutter only for a case of minor practical relevance.

(e) *Continuity.* To show continuity, we have to consider all cases of equal eigenvalues – and therefore undefined eigenvectors – as well as all transitions from real to complex eigenvalues. In 2d, equal real eigenvalues result in a circular glyph, whereas at the transition between real and complex eigenvalues, the glyph is always the characteristic ellipse.

In 3d, the following additional events have to be checked. The first case is the transition from a unique base plane to all positive (or all negative) real eigenvalues: the choice of the blend weights (7) ensures that in the transition event exactly one weight is non-zero, which gives continuity. The other case is the event of equal eigenvalues if all eigenvalues are real and positive/negative: here also only one weight is non-zero, giving continuity.

9.2 A critical review of requirements

The set of requirements determines the glyph design and should be chosen carefully because every desired property constrains the space of admissible glyphs. In the extreme case, this space may even be empty for contradicting requirements. More generally, the imposed conditions may be "too strong" in the sense that the admissible glyphs do not feature an intuitive interpretation anymore. This, however, is crucial in any application of glyphs. In this case, one option is to remove or to relax certain conditions, e.g., demanding only partial fulfillment like "almost everywhere".

We strongly advocate for meeting *all* requirements (a)-(e) for the general design of tensor glyphs: these properties constitute a standard choice that was established by Schultz and Kindlmann [15]. Moreover, Kindlmann and Scheidegger [9] proposed three general visualization *design principles*: representation invariance, unambiguous data representation, and visual-data correspondence. The conditions (a), (b), (d), (e) formally implement these principles and guarantee their fulfillment. Missing in this list is condition (c): the direct visual encoding of real eigenvalues and eigenvectors, if present, seems to be nontrivial. At the same time, this information is of such importance for the characterization of a tensor in essentially every application that condition (c)

appears as an obvious choice for glyph design. For the example of Jacobian matrices of vector fields, the eigenvalues and eigenvectors give a direct classification of the flow around critical points.

For sure, different applications may require emphasis on different properties of the tensor and therefore relax certain conditions in favor of a more intuitive interpretation. However, this holds for the particular application or task and comes at the cost of loosing possibly important parts of the information. For a *generic* glyph design that is not a priory tailored toward a specific application, the theoretically sound and hence "safe" option is to implement *all* conditions (a)-(e). This is not necessarily complicated: In section 8 we give few simple rules on how to read the proposed glyphs. This gives evidence that it is rather easy to learn reading the new glyphs.

Finally, this work focuses on the generic construction of a design space for 2d and 3d glyphs that meet all of the mentioned requirements, which has not been done before. It does neither formally measure the intuitiveness of glyphs nor does it systematically explore this space with the goal of finding glyphs within the constraints that are in some sense "optimal" for a specific application. Possible directions are discussed below.

9.3 Design decisions

The space of all possible solutions to the construction of glyphs fulfilling (a)-(e) is huge. In this paper we give only one sample (and to the best of our knowledge the first one). This raises the question how to further explore the space.

Color schemes. We use a rather straightforward color scheme to encode one continuous value, in 2d this is γ. We do so to ensure comparability with similar approaches [15, 19] that proposed similar colors. Other and in particular more perception-oriented color maps are possible. We remark finally that [15, 19] only use few discrete colors whereas proposition 5.1 states that we have to use a continuous color wheel.

Encoding of eigenvectors. Our approach is based on an encoding of the eigenvectors as discontinuities in the glyph's shape. Even though the human visual system reacts rather sensitive to discontinuities in a shaded scene, perception can be increased by ridge enhancement methods. This makes illustrative techniques interesting candidates for rendering our shapes. The main challenge here is to ensure a smooth cease and disappearance of the enhancements in the case of equal eigenvalues.

Perceptional considerations. Small changes in the tensors should lead to equally small changes in the perception of the glyphs. In order to proceed in this direction, we first need a metric in the space of all tensors, and it seems not at all obvious which one to choose! Only then a study on the perception of the glyphs is meaningful.

Similarity to existing special cases. Another design goal for glyphs could be the similarity to well-established glyphs in special cases, e.g., to Schultz' and Kindlmann's superquadrics [15] for symmetric tensors. Our current approach disregards this goal.

9.4 Comparison with existing techniques

Parallel to this work, Seltzer and Kindlmann developed and published an approach with the same goal: glyphs for general second order tensors [16]. Their construction applies only to the 2d case, seemingly without a straightforward extension to 3d, and we give a comparison with our 2d construction.

Seltzer and Kindlmann use a parametrization of the space of 2d tensors that is similar to the (γ, r)-plane: They span the space in terms of three parameters D, S, R that generate isotropic, traceless symmetric, and antisymmetric parts of the tensor. They similarly factor domain rotations and constrain the Frobenius norm $||\mathbf{T}||_F = \sqrt{D^2+S^2+R^2} = 1$ (instead of the spectral norm as for γ, r), which, after projection, leads to a planar parameter space defined by barycentric coordinates. Given a tensor $\mathbf{T} := \mathbf{J}/||\mathbf{J}||_F$ with $||\mathbf{T}||_F = 1$, the following relations hold for D, S, R in [16] and γ, r:

$$\tan\gamma = \frac{R}{D} \qquad \text{and} \qquad r = 1 - S^2 .$$

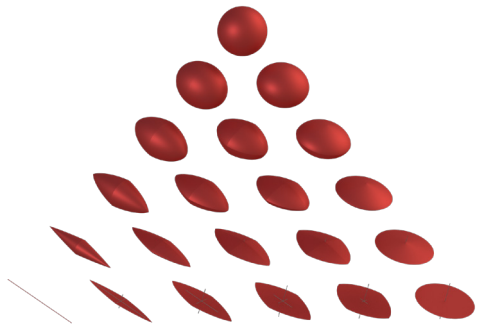

Fig. 10: The proposed glyphs for symmetric positive definite 3d tensors in a similar arrangement as in [8]: In contrast to Kindlmann's superquadric glyphs, the shape discontinuities prevent view-dependent visual ambiguities.

The first equation can be easily verified as follows. In 2d, the polar decomposition of a matrix $\mathbf{J} = \left[\begin{smallmatrix} a & b \\ c & d \end{smallmatrix}\right]$ can be expressed in closed form: find a rotation matrix, parametrized by angle γ, that makes $\mathbf{J}$ symmetric. This leads to $\tan\gamma = \frac{c-b}{a+d}$ and with Eq. (9) in [16] to the above equation. The second equation is already given as Eq. (37) in [16]: in $\det(\mathbf{T}) = 1/2 - S^2$ substitute $r = 1/2 - \det(\mathbf{T})$ from section 4.

Seltzer and Kindlmann give an interpretation of the (D, S, R)-parametrization: $D = 0$ refers to traceless tensors, for $S = 0$ tensors are rotations (without shear or nonuniform scaling) and hence exhibit rotational symmetry, and $R = 0$ refers to symmetric tensors without rotation. In the (γ, r)-space this refers to $\gamma \in \{\pi/2, 3\pi/2\}$ or $r = 0$ and any γ for traceless tensors, $r = 1$ for rotational symmetry, and $\gamma \in \{0, \pi\}$ for symmetric tensors. Finally, the loci of $\det(\mathbf{T}) = 0$ are $S^2 = 1/2$ and $r = 1/2$, respectively. Note that the projection of D, S, R to planar barycentric coordinates is nonlinear, and the projection of the algebraic curve $S^2 = 1/2$ is a conic section rather than a line.

Seltzer and Kindlmann also show – similar to this paper – that shape alone is not sufficient to ensure a unique encoding. Different to this work, they propose a texture on the glyph. This gives an intuitive encoding of the rotation/swirling at the price that continuity and rotation invariance are not completely fulfilled anymore. Furthermore, [16] demand as an ultimate design goal that for the special case of symmetric tensors the well-established superquadric glyphs [8] appear as solution. Our approach is different, and the glyphs differ significantly from superquadric glyphs: Rather than treating symmetry as a special case, our construction always encodes the direction of real eigenvectors (and smoothly changes to left singular vectors in the complex case). [16] lose this property for asymmetric tensors with real eigenvectors.

We finally compare this work to the superquadric glyphs by Kindlmann [8]. This refers to 2d and 3d glyphs, but only for the special case of symmetric positive definite tensors. Figure 10 shows our glyphs in a similar arrangement as in figure 7 in [8]. Note that our solution is different but shares an important design goal: Due to the discontinuities in the shape, there is no visual ambiguity regardless from which perspective the glyph is rendered/viewed. This means that two of the proposed 3d glyphs can *always* be distinguished in the projection to 2d images. In contrast, Kindlmann points out that for his superquadric tensors the 2d projections are not always unique, e.g., in case the 3d glyph is an ellipsoid.

10 Limitations and Future Research

The main theoretical limitation of or approach is the non-uniqueness of 3d tensors of rank 1. We decided not to fix this shortcoming because we consider this case as having only low relevance in practice. A direct road-map for future research comes from the discussion in section 9.3. This includes in particular illustrative or stylized rendering to emphasize relevant information such that visual perception is taken into account *and* all postulated requirements are fulfilled.

APPENDIX

Characteristic ellipse

Given is a tensor $\mathbf{J} \in \mathbb{R}^{2\times 2}$ with rank 2 and *real* eigenvalues $\lambda_{1,2}$ and eigenvectors as columns of $\mathbf{X}$. Its characteristic ellipse is determined by (4).

Proposition 10.1. *The implicit curve defined by* (4) *is an ellipse that interpolates* $\pm\lambda_i \mathbf{X}_{\cdot i}$ *for* $i = 1,2$*, i.e., the eigenvectors scaled by the eigenvalues.*

Proof. The equation $\mathbf{x}^{\mathrm{T}}\mathbf{J}\mathbf{J}^{\mathrm{T}^{-1}}\mathbf{x} = 1$ defines a quadric, i.e., the implicit curve is a conic section [5]. It is indeed an ellipse as $\mathbf{J}\mathbf{J}^{\mathrm{T}}$ is symmetric and positive definite and so is its inverse as $(\mathbf{J}\mathbf{J}^{\mathrm{T}})^{-1} = (\mathbf{J}^{-1})^{\mathrm{T}}\mathbf{J}^{-1}$.

The tensor has spectral decomposition $\mathbf{J} = \mathbf{X}\Lambda\mathbf{X}^{-1}$ with unit length eigenvectors $||\mathbf{X}_{\cdot i}|| = 1$ and singular value decomposition $\mathbf{J} = \mathbf{U}\Sigma\mathbf{V}^{\mathrm{T}}$. We verify that (4) holds for $\mathbf{x}_i = \lambda_i \mathbf{X}_{\cdot i}$ for $i = 1,2$. In matrix notation with $\mathbf{x}_i$ as the two columns of $\mathbf{X}\Lambda$ we write

$$\Lambda\mathbf{X}^{\mathrm{T}}(\mathbf{J}\mathbf{J}^{\mathrm{T}})^{-1}\mathbf{X}\Lambda \;=\; \mathbf{X}^{\mathrm{T}}\mathbf{V}\Sigma\mathbf{U}^{\mathrm{T}}(\mathbf{U}\Sigma^{-2}\mathbf{U}^{\mathrm{T}})\mathbf{U}\Sigma\mathbf{V}^{\mathrm{T}}\mathbf{X} \;=\; \mathbf{X}^{\mathrm{T}}\mathbf{X}$$

using the identities $\mathbf{J}\mathbf{J}^{\mathrm{T}} = \mathbf{U}\Sigma^2\mathbf{U}^{\mathrm{T}}$ and $\mathbf{X}\Lambda = \mathbf{U}\Sigma\mathbf{V}^{\mathrm{T}}\mathbf{X}$, obtained from the factorizations, and then exploiting orthogonality of $\mathbf{U}$ and $\mathbf{V}$. The diagonal entries $\left(\mathbf{X}^{\mathrm{T}}\mathbf{X}\right)_{ii}$ evaluate to 1 and are by construction equal to $\mathbf{x}_i(\mathbf{J}\mathbf{J}^{\mathrm{T}})^{-1}\mathbf{x}_i$, which shows that the equation holds. Obviously, the same holds for $-\mathbf{X}\Lambda$ and hence $-\mathbf{x}_i$. □

Equation (4) holds equally for *non-real* $\pm\mathbf{x}_i \in \mathbb{C}$, $i = 1,2$. However, the interpretation of the ellipse in the real plane (for $\mathbf{x} \in \mathbb{R}$) changes: the complex eigenvectors are "replaced" by the left singular vectors $\mathbf{U}$, which span the orthogonal principal axes, and it is easy to verify that the ellipse interpolates the column vectors of $\pm\mathbf{U}\Sigma$. For $\mathrm{rank}(\mathbf{J}) = 1$, the characteristic ellipse degenerates to a line segment.

Rational parametrization of the characteristic ellipse

The quadric (4) is an implicit representation for the characteristic ellipse, which can be parametrized as a rational quadratic curve [5]. A particularly simple construction is as follows: Express the rational curve in Bernstein-Bézier form as

$$\mathbf{f}(t) = \frac{w_0\mathbf{b}_0(1-t)^2 + w_1\mathbf{b}_1 2(1-t)t + w_2\mathbf{b}_2 t^2}{w_0(1-t)^2 + w_1 2(1-t)t + w_2 t^2}\;,\; t \in [0,1]\;,$$

with control points $\mathbf{b}_i \in \mathbb{R}$. The weights $w_i \in \mathbb{R}$ can always be chosen such that at the end points $w_0 = w_2 = 1$. Figure 2a shows an example.

Assume $\mathbf{J}$ has eigenvalues $\lambda_1 = \lambda_2 = 1$, i.e., $\mathbf{J} = \mathbf{X}\mathbf{I}\mathbf{X}^{-1}$, and construct a parametrization of one arc of the unit circle that is enclosed by the eigenvectors $\mathbf{X}_{\cdot i}$. From end point interpolation of rational Bézier curves the left and right control points $\mathbf{b}_0$ and $\mathbf{b}_2$ are determined as the unit length eigenvectors $\mathbf{X}_{\cdot i}$. The tangents of the curve at the end points are given as tangents to the unit circle or a 90 degree rotation of $\mathbf{X}_{\cdot i}$. End points and tangent directions define two lines, and the center control point $\mathbf{b}_1$ is determined as their intersection. Let α denote angle enclosed by the eigenvectors. It is easy to verify (5), i.e., determine ω in $\mathbf{b}_1 = \omega(\mathbf{b}_0 + \mathbf{b}_2)$: w.l.o.g. use eigenvectors $(\cos(\alpha/2), \sin(\alpha/2))$ to exploit symmetry, and obtain $\mathbf{b}_1 = (\frac{1}{\cos(\alpha/2)}, 0)$, then compare to $\mathbf{b}_0 + \mathbf{b}_2 = (2\cos(\alpha/2), 0)$ to determine the factor $\omega = (1+\cos\alpha)^{-1}$. The weights associated with the three control points are $w_0 = w_2 = 1$ and for the center $w_1 = \cos(\alpha/2)$. For the general construction with unconstrained eigenvalues, i.e., arcs of an ellipse, the control points are transformed linearly as $\mathbf{J}\mathbf{b}_i$ for $i = 0,1,2$. The weights remain unchanged. Due to the affine invariance property of rational Bézier curves, mapping the circular arc results in the same curve as performing the construction directly for a general ellipse. The proposed parametrization can be applied similarly or symmetrically to all four arcs of the characteristic ellipse. Finally, the construction is straightforward for the degenerated case when $\mathrm{rank}(\mathbf{J}) = 1$ (or $\cos\alpha = -1$): in this case $\mathbf{b}_1$ is undefined, however, as $w_1 = \sin\alpha = 0$ the curve is just the line segment spanned by $\mathbf{b}_0$ and $\mathbf{b}_2$.

Surface patches

For the 3d case, we construct surface patches from three quadratic rational boundary curves in Bernstein-Bézier form. Although, three such curves determine a triangular rational quadratic surface patch, such patches are parts of ellipsoids, and in particular spheres, only in special configurations [5]. In general, a rational surface patch of total degree four is required. We follow the construction in [14] that uses a rational bi-quadratic patch that is "degenerated" by the map to the triangle domain. Then the 3×3 control points and weights $(\mathbf{b}_{ij}, w_{ij})$ of the patch are determined as

$$\begin{array}{ccc} (\mathbf{x}_3, 1) & (\mathbf{x}_3, w_{12}) & (\mathbf{x}_3, 1) \\ (\nu_{12}(\mathbf{x}_3+\mathbf{x}_1), \sqrt{2}/2) & (\mathbf{b}_{11}, \sqrt{2}/2\, w_{12}) & (\nu_{12}(\mathbf{x}_2+\mathbf{x}_3), \sqrt{2}/2) \\ (\mathbf{x}_1, 1) & (\mu_{12}(\mathbf{x}_1+\mathbf{x}_2), w_{12}) & (\mathbf{x}_2, 1) \end{array}$$

with the center control point $\mathbf{b}_{11} = \nu_{12}(\mu_{12}(\mathbf{x}_1+\mathbf{x}_2) + \mathbf{x}_3))$, and $\pm\mathbf{x}_i = \lambda_i\mathbf{X}_{\cdot i}$ are scaled eigenvectors. Assume that the boundary curve from $\mathbf{x}_1$ and $\mathbf{x}_2$ is located in the reference plane. This determines the surface patches for the 3d glyph in the case of a well-defined base plane (see section 6) as reference plane, which gives the weight w_{12} and the factor μ_{12} as in the 2d case.

In the case that no base plane can be established, we construct a continuous surface patch by blending the results of the evaluation of the three possible patches. While section 6 discusses and justifies the choice of blend weights, we need to clarify the surface evaluation, which defines a different, non-standard class of surface patch. Let $\mathbf{f}_i : [0,1]\times[0,1] \to \mathbb{R}^3$, $i = 0,1,2$, denote the three rational patches with base curves from $\mathbf{x}_i$ to $\mathbf{x}_{i+1 \bmod 3}$. The core idea is a reparametrization of $\mathbf{f}_i(u,v)$ as $\mathbf{f}_i(\beta_1,\beta_2,\beta_3)$ with barycentric coordinates $\beta_1+\beta_2+\beta_3 = 1$ such that

$$(\beta_1\mathbf{x}_1 + \beta_2\mathbf{x}_2 + \beta_3\mathbf{x}_3) \parallel \mathbf{f}_i(u,v)\;, \tag{8}$$

i.e., the barycentric combination of scaled eigenvectors that span the patch yields a vector that is parallel to the position vector $\mathbf{f}(u,v)$. In this parametrization, we can evaluate the blend patch as

$$\mathbf{f}(\beta_1,\beta_2,\beta_3) \;=\; \frac{1}{\sum_0^2 W_i}\sum_0^2 W_i\,\mathbf{f}_i(\beta_1,\beta_2,\beta_3)\;,$$

using the blend weights W_i defined in (7).

In order to construct the parametrization (8) – w.l.o.g. for $\mathbf{f}_1$ – consider the roots of the norm of the cross product. Due to symmetries, the solution can be expressed as follows. Find $u(\beta_1,\beta_2,\beta_3) \in [0,1]$ as solution of the quadratic equation

$$(1-u)^2 b_0 + 2(1-u)u\,b_1 + u^2 b_2 \;=\; 0\;,$$

for $b_0 = \beta_2$, $b_1 = w_{12}\mu_{12}(\beta_2-\beta_1)$, $b_2 = -\beta_1$. The expression in the quadratic Bernstein polynomials reveals immediately that there exists one solution $u_0 \in [0,1]$. Then find $v(\beta_1,\beta_2,\beta_3) \in [0,1]$ similarly as the root

$$(1-v)^2 c_0 + 2(1-v)v\,c_1 + v^2 c_2 \;=\; 0\;,$$

with $u := u(\beta_1,\beta_2,\beta_3) = u_0$, $\tilde{u} := 1-u$, $\tilde{\beta} := \beta_3 - \beta_1 - \beta_2$, and

$$\begin{aligned} c_0 &= \sqrt{2}\beta_3(\tilde{u}^2 + 4w_{12}\mu_{12}\,u\tilde{u} + u^2)\;,\\ c_1 &= \nu_{12}(\tilde{\beta}\tilde{u}^2 + 2w_{12}(2\mu_{12}\beta_3 - \beta_1 - \beta_2)\,u\tilde{u} + \tilde{\beta}u^2)\;, \text{ and}\\ c2 &= -\sqrt{2}(\beta_1+\beta_2)(\tilde{u}^2 + 2w_{12}\,u\tilde{u} + u^2)\;. \end{aligned}$$

ACKNOWLEDGMENTS

This work was supported by DFG grant TH 692/13-1. The authors would like to thank Gordon Kindlmann for stimulating discussion. The cylinder data set was provided by Tino Weinkauf, the Rayleigh-Bénard convection was simulated with NaSt3DGP. We thank Tobias Günther and Thomas Seidl for help with rendering some pictures and the video. Some pictures were rendered with Amira.

REFERENCES

[1] R. Borgo, J. Kehrer, D. H. Chung, E. Maguire, R. S. Laramee, H. Hauser, M. Ward, and M. Chen. Glyph-based visualization: Foundations, design guidelines, techniques and applications. *Eurographics State of the Art Reports*, pages 39–63, 2013.

[2] P. Crossno, D. H. Rogers, R. M. Brannon, and D. Coblentz. Visualization of salt-induced stress perturbations. In *Proc. IEEE Visualization*, pages 369–376, 2004.

[3] W. C. de Leeuw and J. J. van Wijk. A probe for local flow field visualization. In *Proc. IEEE Visualization*, pages 39–45, 1993.

[4] C. Dick, J. Georgii, R. Burgkart, and R. Westermann. Stress tensor field visualization for implant planning in orthopedics. *IEEE TVCG (Proc. Visualization)*, 15(6):1399–1406, 2009.

[5] G. Farin. *Curves and Surfaces for CAGD*. Morgan Kaufmann, 5th edition, 2002.

[6] A. Globus, C. Levit, and T. Lasinski. A tool for visualizing the topology of three-dimensional vector fields. In *Proc. IEEE Visualization*, pages 33–40, 1991.

[7] R. B. Haber. Visualization techniques for engineering mechanics. *Comput. Syst. Educ.*, 1(1):37–50, 1990.

[8] G. Kindlmann. Superquadric tensor glyphs. In *Proceedings of the Sixth Joint Eurographics-IEEE TCVG conference on Visualization*, pages 147–154, 2004.

[9] G. Kindlmann and C. Scheidegger. An algebraic process for visualization design. *IEEE TVCG*, 20(12):2181–2190, Nov. 2014.

[10] A. Kratz. *Three-Dimensional Second-Order Tensor Fields: Exploratory Visualization and Anisotropic Sampling*. PhD thesis, FU Berlin, 2013.

[11] A. Kratz, C. Auer, M. Stommel, and I. Hotz. Visualization and Analysis of Second-Order Tensors: Moving Beyond the Symmetric Positive-Definite Case. *Computer Graphics Forum*, 2013.

[12] A. Kratz, B. Meyer, and I. Hotz. A visual approach to analysis of stress tensor fields. In H. Hagen, editor, *Scientific Visualization: Interactions, Features, Metaphors*, volume 2, pages 188 – 211. Schloss Dagstuhl–Leibniz-Zentrum für Informatik, 2011.

[13] D. Palke, G. Chen, Z. Lin, H. Yeh, R. Laramee, and E. Zhang. Asymmetric tensor visualization with glyph and hyperstreamline placement on 2d manifolds. 2009.

[14] L. Piegl and W. Tiller. Curve and surface constructions using rational B-splines. *Compututer Aided Design*, 19(9):485–498, Nov. 1987.

[15] T. Schultz and G. L. Kindlmann. Superquadric glyphs for symmetric second-order tensors. *IEEE TVCG*, 16(6):1595–1604, 2010.

[16] N. Seltzer and G. Kindlmann. Glyphs for asymmetric second-order 2d tensors. *Computer Graphics Forum (Proc. EuroVis)*, 35(3):141–150, 2016.

[17] G. Strang. *Introduction to Linear Algebra*. Wellesley-Cambridge Press, 4th edition, 2009.

[18] H. Theisel and T. Weinkauf. Vector field metrics based on distance measures of first order critical points. *Journal of WSCG*, 10(3):121–128, 2002.

[19] H. Theisel, T. Weinkauf, H.-C. Hege, and H.-P. Seidel. Saddle connectors – an approach to visualizing the topological skeleton of complex 3d vector fields. In *Proc. IEEE Visualization*, pages 225–232, 2003.

[20] E. Zhang, H. Yeh, Z. Lin, and R. S. Laramee. Asymmetric tensor analysis for flow visualization. *IEEE TVCG*, 15(1):106–122, 2009.